ELSEVIER

Contents lists available at ScienceDirect

Sensors and Actuators: A. Physical

journal homepage: www.journals.elsevier.com/sensors-and-actuators-a-physical



Hierarchical rotating-bending metamaterials for simultaneous mechanical vibration suppression and electricity generation

Ramin Hamzehei ^a, Mahdi Alaei Varnosfaderani ^c, Mahdi Bodaghi ^{b,*}, Nan Wu ^{a,*}

- a Department of Mechanical Engineering, University of Manitoba, Winnipeg, Manitoba R3T 5V6, Canada
- ^b Department of Engineering, School of Science and Technology, Nottingham Trent University, Nottingham NG11 8NS, UK
- ^c Department of Civil Engineering, University of Manitoba, Winnipeg, Manitoba, R3T 5V6, Canada

ARTICLE INFO

Keywords: Piezo elements Vibration isolation Electricity generation Quasi-zero stiffness 3D printing

ABSTRACT

This study introduces a hierarchical metamaterial with a rotating-bending mechanism, featuring high-stiffness triangular joints between dodecagon unit cells. The proposed structure is additively manufactured from thermoplastic polyurethane (TPU) and further analyzed through finite element analysis (FEA) to explore the deformation mechanisms. Under compression, the high-stiffness triangular joints rotate, inducing bending in adjacent walls, resulting in enhanced stability and quasi-zero-stiffness (QZS) features. Local deformation mechanisms include pure bending, bending combined with shear, and simultaneous shrinkage and expansion. To harness these local deformations, piezo elements integration strategies are proposed. A piezo bender (PB) is adhered to regions experiencing pure bending, lead zirconate titanate (PZT) patches are attached where bending and shear coexist, and piezo stacks are applied at locations with shrinkage and expansion. Experimental results show that before and after gluing piezo elements, the structure exhibits obvious vibration isolation performance, which is independent of the number of unit cells. From the frequency transfer functions, at 10 Hz, where vibration isolation arises, the PB and piezo stack generate power around 8.6 and 2.6 $\frac{\mu W}{g}$, respectively, while PZT generates power around 11 nW/g. At a higher frequency of 200 Hz, the PB generates a power of 32 nW/g, piezo stack generates a power of 7.6 nW/g, and PZT generates a power of 2.9 nW/g. The proposed hierarchical metamaterials provides multifunctional capabilities, simultaneously isolating vibrations and generating electricity. They facilitate versatile solutions in vibration/stiffness control of engineering structures, like wearable devices, home appliances, vehicle parts, and civil infrastructures, by providing self-powered sensing and energy generation ability.

1. Introduction

Mechanical metamaterials are man-made structures engineered to possess unique mechanical characteristics through their precisely designed internal geometries [1]. Unlike traditional materials, the mechanical behaviour of lattice structures arises from geometry rather than material composition, offering exceptional design flexibility and customization for specific functions. They can display unusual properties such as negative Poisson's ratio [2], negative stiffness [3], negative thermal expansion [4], and tunable mechanical properties like adjustable stiffness [5].

Mechanical metamaterials can be broadly categorized based on the geometry and topology of their unit cells. Common types include truss-based lattices [6], which consist of interconnected straight beams and

are widely used for their high strength-to-weight ratios. Plate-based lattices [7] incorporate thin-walled surfaces or sheets as structural members, offering improved energy absorption under impact. Shell-based or curved lattices [8,9] feature non-linear beam or wall geometries, enabling localized deformation and better adaptability under complex loads. Re-entrant lattices [10], characterized by inward-pointing angles, are well known for their negative Poisson's ratio. In contrast, chiral and anti-chiral lattices [11,12] use tangential connections and rotational symmetries to produce auxetic effects, often showing directional mechanical responses. To improve the performance of lattice structures, hierarchical metamaterials [13] have been proposed and developed. In these structures, smaller-scale repeating patterns of internal design are placed inside the main unit cells, creating multiple levels of hierarchy in geometry. Each of these lattice types

E-mail addresses: mahdi.bodaghi@ntu.ac.uk (M. Bodaghi), nan.wu@umanitoba.ca (N. Wu).

^{*} Corresponding authors.

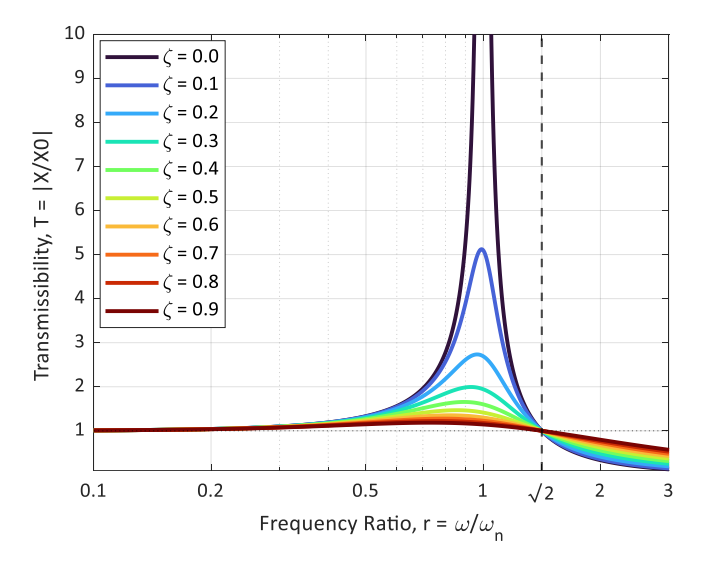


Fig. 1. Transmissibility curve of a damped SDOF system at various damping ratios, with $\frac{w}{w} = \sqrt{2}$ indicating the onset of the isolation region.

serves specific functional purposes depending on the application and loading conditions.

When it comes to functionality, mechanical metamaterials can generally be divided into two categories, so-called passive [14] and active metamaterials [15]. Passive metamaterials derive their unusual mechanical behaviour purely from their geometric structure and base material without any need for an external energy source to operate. In contrast, active metamaterials rely on smart materials, substances that change their properties in response to external stimuli like voltage, temperature, pressure, or electric and magnetic fields. Examples of smart materials include shape-memory polymers [16] and alloys [17], regaining their original shape when heated, magneto-rheological materials [18], altering their viscosity in magnetic fields, and piezoelectric materials [19], producing an electrical charge once a mechanical load is applied. When integrated into passive metamaterials, these smart materials enable the creation of multi-functional active metamaterials, which can respond based on specific external stimuli and the existence of specific smart materials. Consequently, thanks to the customizable architectural design and functionality of metamaterials, they can be used for a variety of applications, including energy absorption [20,21], sound insulation [22,23], impact resistance [24,25], vibration attenuation [26,27] and electricity generation [28,29].

From an engineering standpoint, mechanical vibration refers to the oscillation of an object around a stable point [30]. The vibration behaviour is largely influenced by the system's stiffness and its natural frequency, which is calculated using the formula $\omega_n = \sqrt{\frac{k}{m}}$, where "K" is stiffness and "m" is mass of the system, respectively. A higher stiffness leads to a higher natural frequency, vice versa. Another key concept is the frequency ratio, which is the ratio of excitation frequency to natural frequency. The graph in Fig. 1 illustrates the transmissibility of a damped single-degree-of-freedom (SDOF) system for various damping ratios. As the damping ratio increases, the resonance peak decreases, and the system becomes less sensitive to excitation near its natural frequency. The vertical line at $\frac{w}{w_n} = \sqrt{2}$, marks the onset of the isolation region, beyond which vibration transmission falls below unity. This demonstrates the limitation of linear isolators and highlights the motivation for developing QZS systems capable of achieving isolation at lower frequency ratios.

Mechanical metamaterials are gaining attention for their effectiveness in vibration isolation [31], especially those employing QZS designs [32–43]. Pan et al. [32] integrated a QZS mechanism with a rotational structure to overcome the poor load-bearing capacity that occurs in

common vibration isolators. Their design shows vibration isolation behaviour within a wide range of 5-300 Hz. Liu et al. [33] proposed a novel design of metamaterial showing simultaneous multi-directional QZS and vibration attenuation properties at low frequencies. Li et al. [34] proposed a novel QZS design, combining PS and NS elements, for simultaneous vibration isolation with ultra-wideband and energy absorption applications under cyclic loadings. Wu et al. [35] introduced a tunable load-adaptive QZS metamaterial for low-frequency vibration isolation. Their design can be customized to tolerate different loads without any need for refabrication. Liu et al. [36] developed cylindrical springs using a modular design that allows for a customizable QZS feature. By combining specially designed unit cells with adjustable stiffness, they achieved tunable low-frequency vibration isolation. Dalela et al. [37] designed a tunable QZS metamaterial using just a single flexible beam. Their approach relies on the beam's buckling behaviour to create QZS properties for isolating low-frequency vibrations. Liu et al. [38] proposed a novel design approach to exhibit simultaneous stability and multi-QZS regions exhibiting varying loads. Huo et al. [39] proposed a novel mechanical metamaterial that arranges OZS units in a Cartesian layout using curved beams and developed a dynamic model to evaluate its response under base excitation. Their design showed a low-frequency vibration isolation feature caused by elastic buckling. Ma et al. [40] proposed a novel design approach possessing a customizable QZS feature achieved by porosity factor and unit size for low-frequency vibration isolation via inverse design. Zhang et al. [41] proposed a novel QZS mechanism for low-frequency vibration caused by pre-shaped cosine-based ligaments. Their design showed a reduction in peak resonance compared to the nonlinear vibration isolators. Xu et al. [42] designed a W-shaped metamaterial on a small scale that possesses both a QZS feature and a vibration isolation feature at low frequencies. Their design provided a friendly fabrication without any need for assembly and was easy to miniaturize. Zhang et al. [43] developed tailored mechanical metamaterials with programmable QZS features using curved beam geometries to achieve multiple QZS working ranges. Their design demonstrated tunable stiffness and effective ultra-low-frequency vibration isolation through structural programming.

Apart from QZS property and vibration isolation behaviour that metamaterials possess, they can be used for energy harvesting and electricity generation applications [44-55]. Zhang et al. [44] proposed a novel piezoelectric energy harvester by integrating a rotating triangular auxetic structure into a cantilever beam. This design enhances the average stress in the piezoelectric patch, introduces negative Poisson's ratio effects, and significantly improves output power and bandwidth for harvesting low-frequency vibrations. Mortazavi et al. [45] proposed an arc-shaped auxetic cantilever beam energy harvester under moving mass excitations using re-entrant structures to improve low-frequency vibration harvesting. Bolat et al. [46] showed that auxetic beams, especially with non-traditional geometries, demonstrated enhanced energy harvesting potential under various vibration conditions, including forced vibration and wind-induced galloping. Zhang et al. [47] designed a peanut-shaped auxetic piezoelectric energy harvester with a sliding proof mass, achieving frequency self-tuning, enhanced power output, and a significantly wider working bandwidth under ambient vibrations. Ravanbod et al. [48] proposed a perforated reentrant-chiral honeycomb auxetic structure for ultra-low-frequency piezoelectric energy harvesting. Their design leveraged stress concentration, geometric tuning, and strain controllability to outperform conventional auxetic harvesters. Megdich et al. [49] developed a 3D-printed composite multimodal auxetic structure based on Polyvinylidene fluoride/multi-walled carbon nanotubes (PVDF/MWCNTs) composites that activate multiple piezoelectric modes to achieve high output voltage. Ichige et al. [50] optimized the geometric dimensions of a metamaterial elastic layer in a piezoelectric vibrational energy harvester to achieve significantly enhanced power generation and reduced resonance frequency while maintaining fabrication simplicity. Zhao et al.

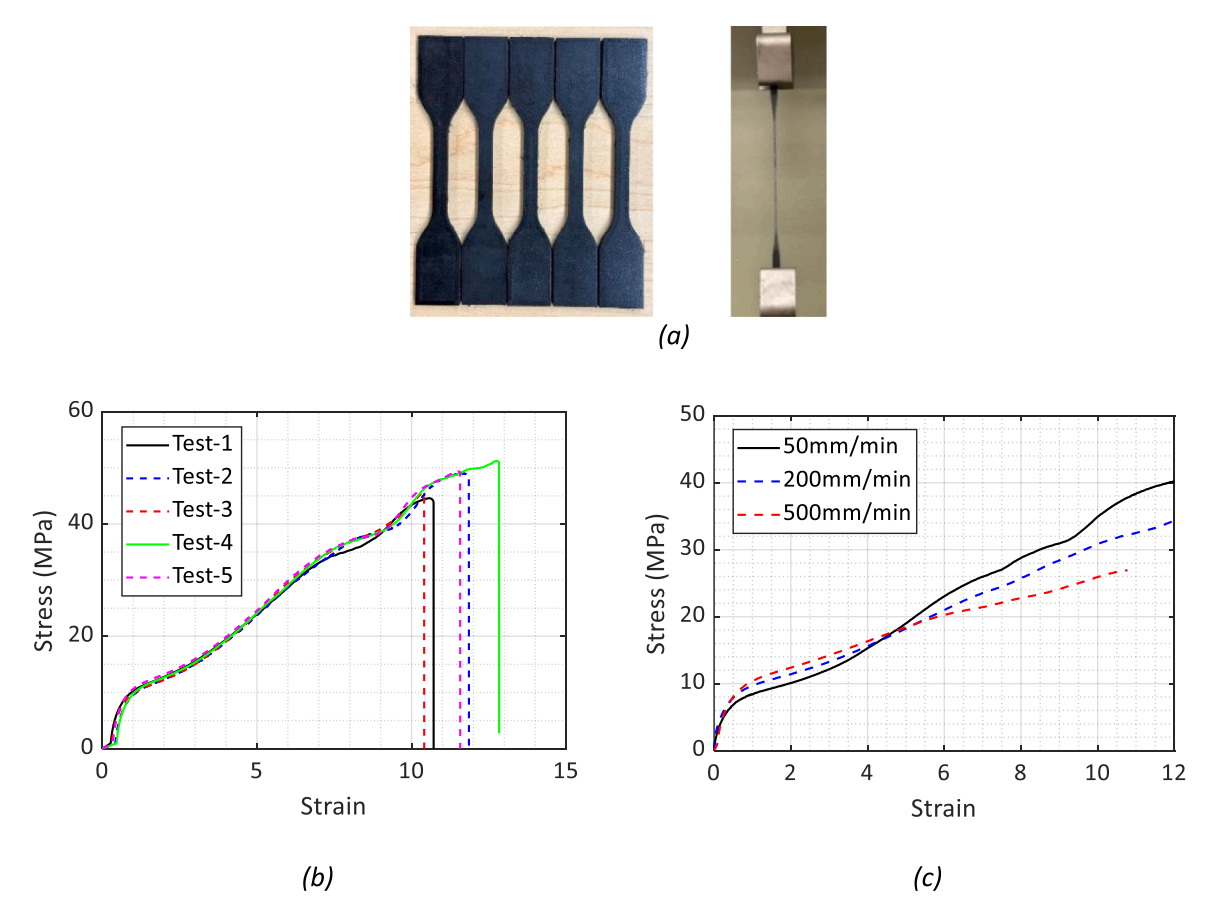


Fig. 2. (a) 3D-printed TPU samples with corresponding tensile test, (b) stress-strain curves of TPU at 50 mm/min, and (c) strain independence behaviour of TPU at different speeds.

Table 1 Printing parameters.

Printing parameters	Value
Nozzle diameter	0.4 mm
Nozzle temperature	250°C
Bed temperature	30°C
Printing speed	50 mm
Infill direction	± 45
Infill percentage	100 %

[51] developed a viscoelastic metamaterial beam with integrated vibration isolation and energy harvesting, which utilizes nonlinear resonators to concentrate vibrational energy and significantly enhance damping and energy output within the local resonance band gap. Fang et al. [52] introduced an auxetic nonlinear vortex-induced vibration energy harvester that combines monostable magnetic softening and auxetic geometry to enhance energy harvesting efficiency, especially under varying low wind speeds, outperforming conventional nonlinear designs. Mortazavi et al. [53] investigated energy harvesting from moving mass-induced vibrations using auxetic cantilever beams, demonstrating that the double arrowhead auxetic design achieved superior power output under bridge simulator excitations. Chen et al. [54] proposed a plucking rotational energy harvester enhanced by auxetic structures and tapered thickness, achieving a power output up to 898 % higher than that of conventional counterparts under low-frequency

rotations. Wang et al. [55] demonstrated that integrating auxetic beams into hybrid systems is a promising strategy for boosting power output in low-frequency vibration energy harvesting. Liu et al. [56] proposed a device containing four piezoelectric buckled beams and a vertical spring for vibration isolation and energy harvesting. Their design exhibited negative stiffness behaviour in the vibration direction, resulting in vibration isolation at low frequencies, while simultaneously generating large stress and strain on the piezo elements to produce a high electrical output. In addition, Liu et al. [57] employed the concept of 1:2 internal resonance by designing a structure that contains a pendulum suspended beneath a spring-supported platform, with a magnet mounted at its tip that interacts with multiple fixed solenoids to enable energy conversion. Their results showed that a 1:2 internal resonance between the platform's vertical motion and the pendulum's swing enables energy transfer, reducing platform vibration while enhancing the pendulum's motion for simultaneous energy harvesting.

While several studies have explored vibration isolation and enhanced energy harvesting using lattice structures, challenges remain in achieving vibration isolation at low frequencies with higher output power. Moreover, most research has focused on energy harvesting of cantilever beam-based metamaterials, which can restrict the integration of multiple piezo elements. This study proposes novel hierarchical triangular-based metamaterials for simultaneous vibration isolation and electricity generation. The proposed design is based on the rotational motion of the triangular joints under compression and bending of the adjacent walls of the unit cells [58]. This leads to a tunable QZS property

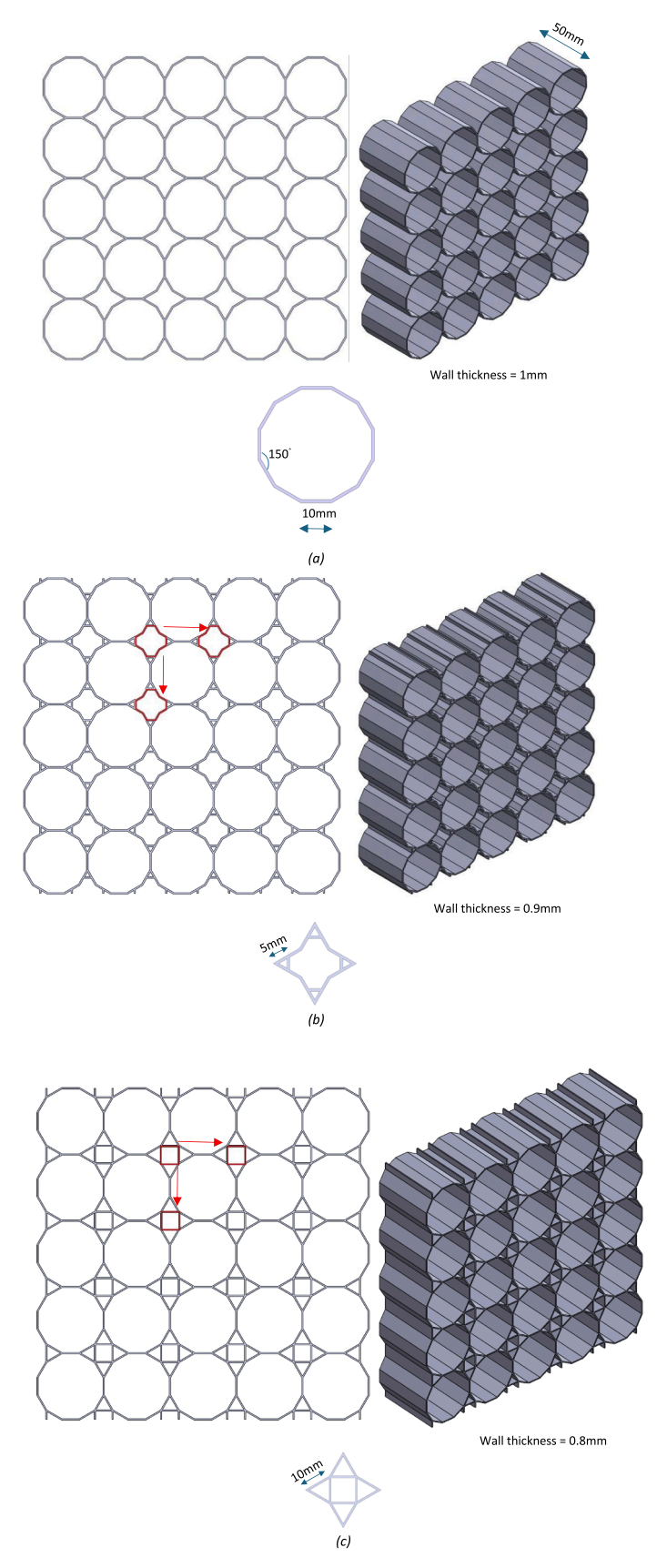


Fig. 3. (a) Dodecagon metamaterial, hierarchical metamaterial with (b) small, and (c) large equilateral triangular joints.

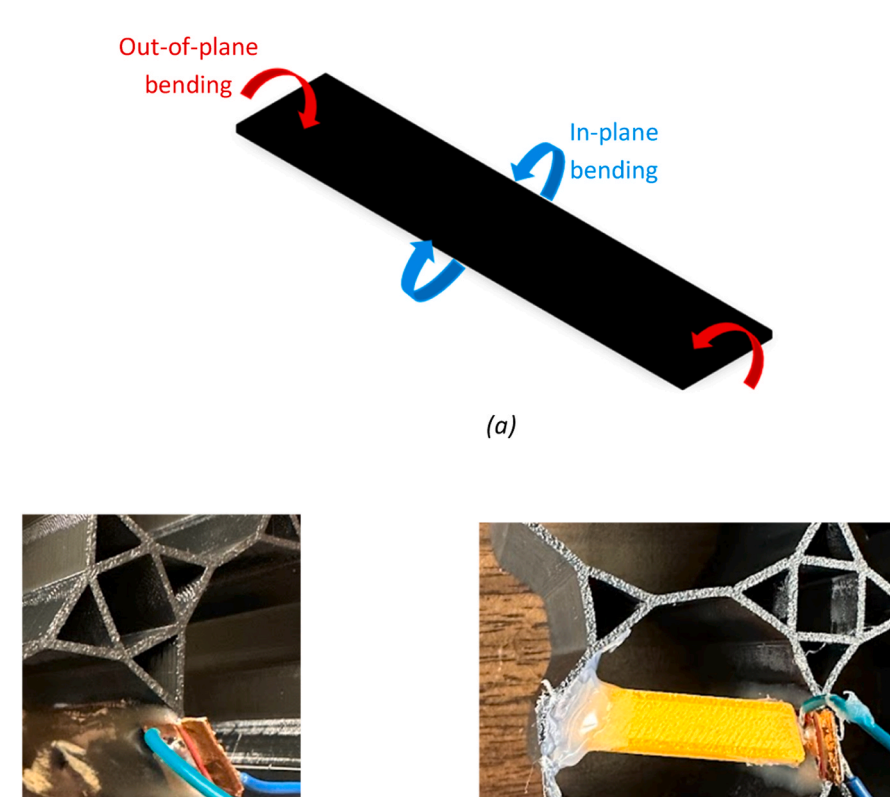


Fig. 4. (a) Schematic of different bending in PB, (b) in-plane bending, and (c) out-of-plane bending via a 3D-printed PLA lever.

for the metamaterial, meaning that the QZS level of the metamaterials is adjustable based on the dimensions of the triangular joints. The smaller the triangles, the higher the QZS level; vice versa. Because of the rotation-bending mechanism occurring during compression, some local mechanisms exist within the metamaterial. They include pure bending, bending-shear, and simultaneous shrinkage-expansion mechanisms. Based on these local mechanisms, some piezo elements, including piezo bender, piezo stack, and lead zirconate titanate (PZT), are glued to the metamaterial and generate reasonable power under external excitations, while a mass is supported on top of the metamaterial. Therefore, the proposed hierarchical triangular metamaterial in this research is multifunctional and exhibits a capability of simultaneous vibration isolation at low frequencies (from 10 Hz onwards) and electricity generation.

(b)

2. Material & methods

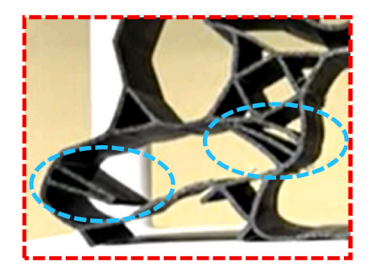
2.1. Material and manufacturing

This study uses TPU as a hyperelastic material [59] for fabrication, characterized by its ability to undergo large elastic deformations and return to its original shape upon removing the applied load. The main reasons for the selection of TPU are related to its flexibility to handle significant bending deformations. To achieve the mechanical properties of TPU, five dog-bone samples were additively manufactured according to the standard ASTM-D-638–14 [60], see Fig. 2a. Tensile tests were carried out by the MTS universal testing machine at a speed of 50 $\frac{mm}{\min}$ based on the ASTM standard, see Fig. 2a. The stress-strain curves of TPU are provided in Fig. 2b. For the fabrication of the samples in this study,

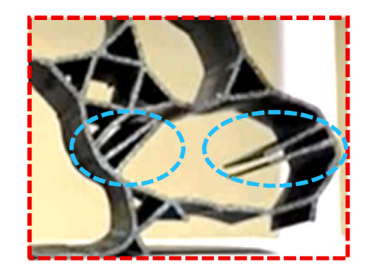
the Bambu Lab X1 carbon 3D printer was employed with the following setup, see Table 1. As TPU is a hyperelastic material and may exhibit strain rate dependency at different mechanical conditions, tensile tests at different speeds of 50, 200, and $500 \, \frac{mm}{min}$ were carried out. Based on the experimental data provided in Fig. 2c, in the low to moderate strain range (0–0.5), which corresponds to the operational regime for vibration isolation under small cyclic displacements, the response is nearly rate-independent. This validates its suitability for vibration isolation testing in this research, where displacement amplitudes and frequencies remain within the domain of small-to-moderate strain.

2.2. Lattice design concept

The structural design of the proposed metamaterials for vibration isolation and energy generation is directly from a dodecagon (12-sided polygon) metamaterial, see Fig. 3a, which is more flexible compared with the previously studied octagonal cells [58], demonstrating the obvious high-stiffness joints' effect on the global negative Poisson's ratio mechanical behaviour. In the following, hierarchical metamaterials are designed according to the repetition of semi-dodecagon and joint supports shown in red colour in Fig. 3b and c. This leads to the tessellation of high-stiffness triangular joints within the metamaterial. Compared with the regular dodecagon honeycomb structure, incorporating the stiffener joints between dodecagonal cells will enhance the structural stability with different local deformation mechanisms caused by a rotating-bending mechanism. This makes the structure suitable for piezo elements embedding for multi-functional applications, including energy generation and realizing the QZS property for vibration isolation. Slightly adjusting the support sizes at the joints will lead to significant



Bending and shear mechanisms



Bending and shear mechanisms

(a)

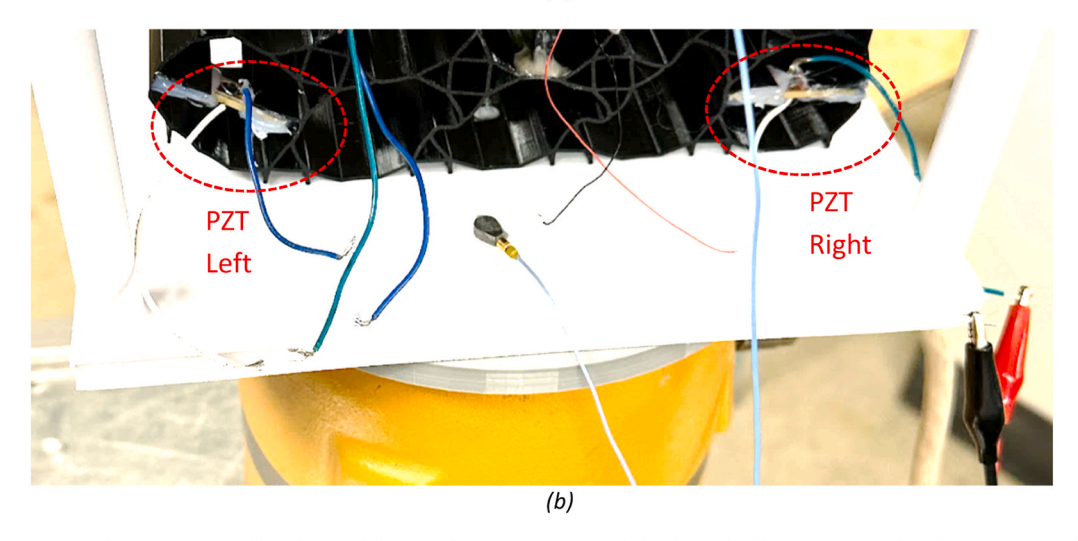


Fig. 5. (a) the coexistence of bending and shear under compression, and (b) the embedding of PZTs within the metamaterial.

mechanical behaviour variation so as to tune the vibration isolation capacity by providing different QZS levels and plateau stages. The corresponding deformation mechanisms and features of the proposed hierarchical metamaterials will be elucidated in the "Results and Discussion" section, based on both finite element analysis (FEA) and experimental results.

2.3. Piezo elements integration

This section outlines the rationale behind selecting specific piezoelectric elements and describes their integration into the large triangular metamaterial. While piezo elements can be embedded in various unit cells, those located near the shaker, where external excitations are most intense, are preferred. Since the hierarchical metamaterial is designed for vibration isolation, certain unit cells exhibit partial or complete isolation, making them unsuitable for energy generation. The underlying principle is that greater excitation leads to higher energy output. The selected piezo elements align with regions exhibiting specific local deformation mechanisms under compressive loading, as detailed below.

2.3.1. Piezo bender (PB)

As reflected from its name, PB generates electricity once a bending force is applied to it. PB has a dimension of $50 \times 10 \times 0.8$ mm. Since it is in a thin rectangular shape, two bending deformations can happen, so-called in-plane and out-of-plane bending, see Fig. 4a. For in-plane bending, it is directly attached to the lattice cell wall at a point where the maximum bending deformation is observed, see Fig. 4b. For out-of-plane bending, the bending force is applied via a 3D-printed PLA lever glued to the wall front, see Fig. 4c.

2.3.2. Lead zirconate titanate (PZT)

PZT generates electricity when subjected to mechanical strain, especially under tensile loads. In the shown lattice structure, the coexistence of bending and shear deformation can create localized tensile strains, which are suitable for PZT patches to generate electricity, see Fig. 5a. In addition, the 3D-printed thin surface areas, shown in blue-dashed ellipses in Fig. 5a, are suitable for bonding the PZT within the metamaterial and transferring localized tensile strain to the PZT.

2.3.3. Piezo stack

The integration of a TPU-based fixture within the tensile-compression dominated zone (as shown in Fig.6) allows for strategic placement of the piezo stack where axial load is applied on it. When the hierarchical metamaterial is compressed, the local unit cell walls bend, creating regions where one side experiences tension and the opposite side experiences compression, see Fig. 6a, transferring direct axial compression to the piezo stack, see Fig. 6b and c. This axial compressive strain is ideal for a piezo stack to generate electricity when compressed along its poling direction. Fig. 6d shows all embedded piezo elements used in this research within the hierarchical metamaterial.

2.4. Finite element analysis

The quasi-static mechanical behaviour of the proposed dodecagon and hierarchical metamaterials is simulated with the help of ABAQUS finite element software. The sixth-order Ogden model was adopted as the hyperelastic constitutive model. The analysis was conducted in two sequential steps: a "linear perturbation buckling" step, followed by a "general static Riks" step. In the buckling analysis, a subspace eigen solver was employed to extract the first five eigenmodes. The first

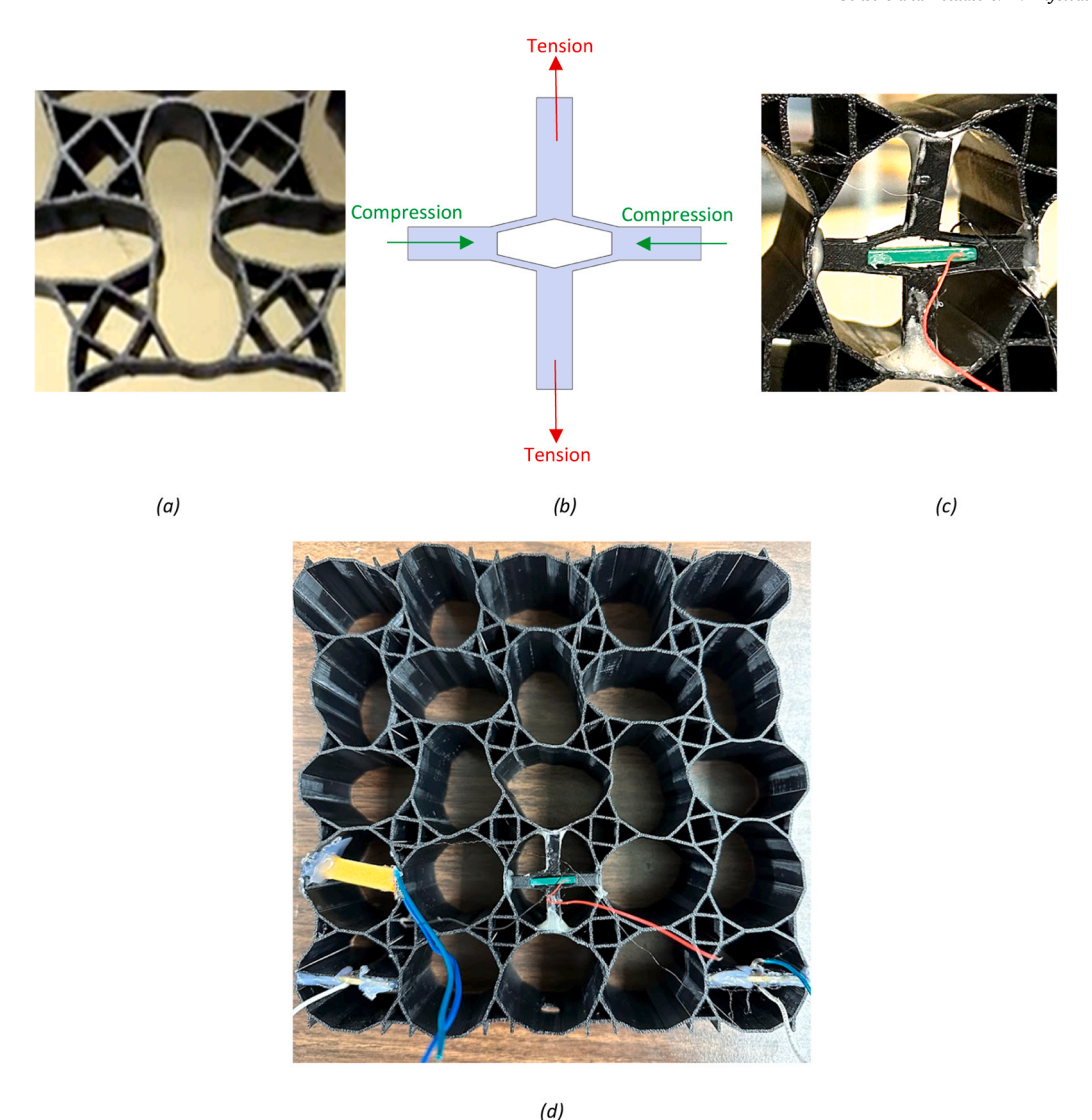


Fig. 6. (a) Localized compressed-extent zone, (b) inner TPU-based fixture for holding piezo stack, (c) glued fixture with embedded piezo stack, and (d) all glued piezo elements within the hierarchical metamaterial.

buckling mode was subsequently introduced as a geometric imperfection into the structure for the Riks step to capture post-buckling and nonlinear deformation behaviour. To implement this imperfection, the buckling mode shapes must first be linked to nodal displacements by adding the following two lines to the model keywords:

*Node file

U

The model is then duplicated in ABAQUS, and the analysis step is changed from "Buckle" to "Static, Riks". After removing the previously added lines, the following command is inserted to apply the imperfection:

*Imperfection, File=Buckle analysis job-name, Step= 1 1, scale-factor

where scale-factor represents a small value (For example, 0.01–0.1) used to scale the first buckling mode shape, and a scale factor of 0.1 was considered for the FEA. For boundary conditions, the movement of the bottom faces of the structures is restricted along the horizontal and vertical directions, and a 15 mm displacement is applied to the top faces, see Fig. 7. The simulations employed C3D8H elements, which are 8-node linear brick elements with a hybrid formulation designed specifically for nearly incompressible materials such as TPU. Unlike reduced integration elements, C3D8H uses full integration but incorporates a hybrid approach to effectively manage pressure constraints. This element

ensures numerical stability during large deformation analyses and is well-suited for simulating complex behaviours such as buckling and post-buckling. The hybrid formulation is particularly advantageous when using static analysis procedures like the Riks method, providing reliable results for highly deformable, incompressible materials. It is worth noting that a mesh study was carried out, and it was shown that a seed size of 0.4 mm, corresponding to half the wall thickness, was used to ensure FEA accuracy, as illustrated in Fig. 11d.

2.5. Experimental set-up

The experimental procedure in this study relies on three main experiments, including a quasi-static compression test to evaluate the stiffness and the QZS property of all lattice structures. Then, a vibration test is carried out to evaluate the vibration isolation behaviour, and simultaneously, the amount of generated voltage by PB, PZT and piezo stack is measured. The details regarding each step are provided in the following subsections.

2.5.1. Quasi-static compression test

To evaluate the mechanical properties of the proposed metamaterials, a quasi-static compression test was carried out at a speed of 5 $\frac{mm}{\min}$ via the MTS universal testing machine, see Fig. 8.

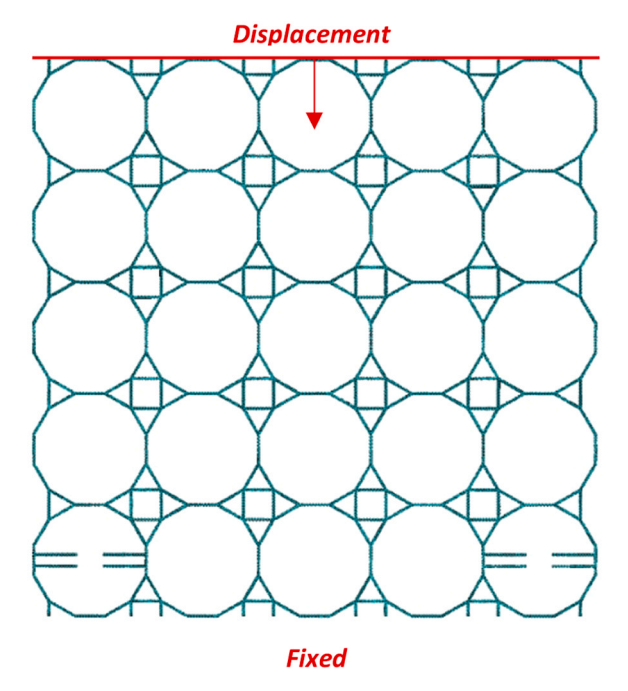


Fig. 7. The meshed sample with corresponding boundary conditions.



Fig. 8. Quasi-static compression test.

2.5.2. Vibration test

A vibration test was carried out via an LDS acoustic shaker with a frequency range of 0–200 Hz, manufactured by Ling Dynamic Systems (LDS), see Fig. 9a. The hierarchical metamaterial with high-stiffness large triangular joints is placed between a 3D-printed PLA fixture, see Fig. 9b. The data acquisition and signal generation system contain a Siemens LMS SCADAS Mobile integrated with LMS Test Lab software. The LMS system is configured to measure the outputs, including generated voltages and accelerations. Accelerations of the base and top plates are captured by two accelerometers, see Fig. 9b, which sends the data to the LMS system for analysis.

2.5.3. Electricity generation test

We employed three piezoelectric materials for energy generation: piezo bender (PB), Lead zirconate titanate (PZT) and piezo stack. PB is a BA5010 piezoelectric bimorph actuator [61] with a dimension of $50 \times 10 \times 0.8$ mm with a capacitance of 97 nF. It is indeed a piezoelectric bimorph configured in parallel poling. These actuators can be wired in either a two-wire or three-wire configuration. For energy generation purposes, we used the two-wire configuration, with the ground connected to the top and bottom electrodes (external surfaces) and the voltage lead connected to the middle plate. In this setup, we utilized the actuator in reverse, operating as an energy generator rather than in its typical actuation role. Energy generation occurs through both in-plane and out-of-plane bending. The in-plane bending occurs where maximum local bending deformation happens, see Fig. 4b. The out-of-plane bending occurs via a 3D-printed lever made from PLA, as illustrated in Fig. 4c. This generates voltage and induces electric fields along with the thickness (polling direction) of PB.

Regarding PZT, two PZTs with a dimension of $40 \times 10 \times 1$ mm with a capacitance of 5.62 nF are embedded and glued in the bottom part of the hierarchical metamaterial, see Fig. 5. To embed a piezo stack, an inner fixture is designed and 3D-printed using the same flexible TPU, see Fig. 6c. Its primary role is to transmit compressive deformation normally onto the piezoelectric stack during structural compression. Fig. 10 shows all the piezo elements used in this research. It is worth mentioning that the details of deformation mechanisms will be discussed in the "Results and discussion" section.

2.5.4. Theoretical maximum generated power

In synchronized energy harvesting systems, energy is extracted in coordination with the mechanical movement of the piezoelectric transducer. Ideally, this extraction happens at each voltage peak, once during the positive half of the vibration cycle and once during the negative half. The energy stored in the piezoelectric generator at each peak can be calculated using Eq. (1) as follows.

$$E_{PEH} = \frac{1}{2} C_p V_{\text{max}}^2 \tag{1}$$

Where C_p and $V_{\rm max}$ are the capacitance and the peak voltage of the piezoelectric, respectively. Assuming the system is being excited at a frequency of f (the number of cycles per second is f). Therefore, the maximum average power (also referred to as raw power) that can theoretically be extracted from the piezoelectric generator [62] is as Eq. (2)

$$P_{PEH,\text{max}} = f.2 \times E_{PEH} = C_p f V_{\text{max}}^2$$
 (2)

3. Results & discussion

The results are presented in two separate sections, including quasistatic and dynamic behaviour. In the quasi-static section, the deformation patterns of hierarchical metamaterial containing large triangles are investigated first by the experiment and validated FEA, then the deformation patterns of dodecagon and hierarchical metamaterials with small triangles are evaluated by FEA. In the following, the vibration behaviour and generated electricity of hierarchical metamaterial with large triangles, embedded with piezo materials, are evaluated experimentally. It is worth noting that two video files, called "Video_1" and "Video_2", showing the vibration isolation behaviour of the metamaterial from different views can be found in the "Supplementary Materials" section.

3.1. Quasi-static compression test

Once compression is applied, the high-stiffness triangular joints rotate first, resulting in bending of the adjacent walls, leading to a global negative Poisson's ratio behaviour, see Fig. 11a. The onset of joints rotation and bending of the walls leads to a softening behaviour and the

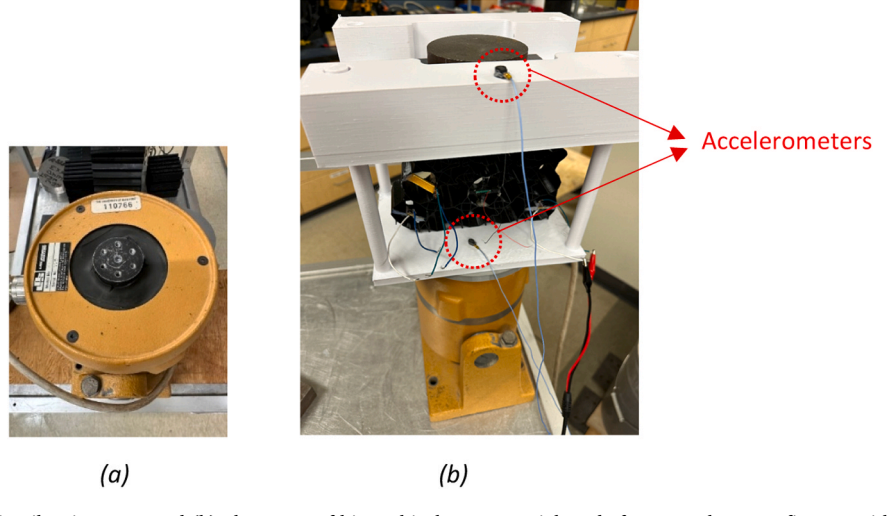


Fig. 9. (a) LDS shaker used in vibration tests, and (b) placement of hierarchical metamaterial made from TPU between fixtures with accelerometer attachment.

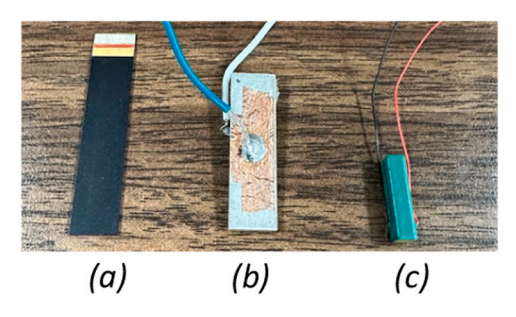


Fig. 10. Different kinds of piezo elements (a) PB, (b) PZT, and (c) piezo stack.

structure's yield. This indeed results in a quasi-zero-stiffness (QZS) behaviour in hierarchical triangular metamaterials. Therefore, the natural frequency of the system decreases ($\omega_n = \sqrt{\frac{k}{m}}$), and frequency ratio increases $(\frac{\omega}{\omega})$. This makes the proposed metamaterials in this study suitable for vibration isolation applications. Due to the existing rotationbending mechanisms, there are some locally available mechanisms, as highlighted in Fig. 11b. As in the green-dashed region the most bending deformation occurs, PB is glued to the metamaterial in this location, see Fig. 11a. The red-dashed regions exhibit the simultaneous bending and shear mechanisms, which are suitable for PZT attachment, see Fig. 11b. The blue-dashed region shows the simultaneous expansion and shrinkage, and this enables applying axial forces on the piezo stack to generate electricity, see Fig. 11b. It is also worth mentioning that there is an excellent coincidence between FEA and experiment, as shown in Fig. 11c and d, and the noises that appeared in the experiment are related to the softness of TPU.

3.2. Tunable QZS property

Fig. 12 shows a schematic representation of double half-length ligaments in the metamaterial structure subjected to equal and opposite end moments "M". The variable "N" shows the adjacent ligament lengths between the two triangular joints, the thickness "t", and the width "b" are modelled as a slender beam with rotational deformation.

From the mechanics of materials point of view [63], when a beam is subjected to pure bending, the curvature is given by Eq. (3). Where "p" is the radius of curvature of the beam, "E" is Young's modulus of the base material, and "I" is the second moment of area of the ligament's cross-section, given by Eq. (4).

$$\frac{1}{\rho} = \frac{M}{EI} \tag{3}$$

$$I = \frac{1}{12} \quad bt^3 \tag{4}$$

Under bending, each small segment of the beam of original length "dx" subtends a small angle " $d\theta$ " at the centre of curvature. By using the definition of arc length, the relation between "dx" and " $d\theta$ " is based on Eq. (5). Substituting Eq. (5) into (3) gives Eq. (6).

$$dx = \rho d\theta \tag{5}$$

$$\frac{d\theta}{dx} = \frac{M}{EI} \tag{6}$$

By integrating along the beam of length "N" gives the total change in slope as in Eq. (7). Because each end rotates almost equally but in opposite directions, as shown in Fig. 12, the rotation at each end is calculated based on Eq. (8). Substituting Eq. (4) into (8) relates the rotational displacement of the joints to the geometrical parameters "N", "b", and "t", and gives Eq. (9). The rotational stiffness of the joints, K_{θ} , is calculated as in Eq. (10), saying that rotational stiffness is inversely related to ligament length "N" ($K_{\theta} = \frac{1}{N}$). This means that the larger the triangular joints, the shorter the length of "N" between the two triangular joints, meaning that higher structural stiffness is achieved when large triangular joints are embedded.

$$\Delta \theta = \int_0^N \frac{M}{EI} dx \tag{7}$$

$$\Phi = \frac{\Delta \Theta}{2} = \frac{MN}{2EI} \tag{8}$$

$$\Phi = -\frac{6MN}{Eht^3} \tag{9}$$

$$K\Theta = \frac{M}{\Phi} = \frac{Ebt^3}{6N} \tag{10}$$

Regarding QZS level, Fig. 13 shows that the hierarchical metamaterial with small triangles shows a higher force level for QZS and lower stiffness compared to the large triangular metamaterial. Indeed, the larger the triangles, the higher the stiffness, the earlier the yield, and the lower the QZS level. On the other hand, the design with smaller triangles makes the structure more flexible, but it can hold a larger mass for vibration isolation at its QZS stage. While, the regular dodecagon metamaterial exhibits a monotonic increase in force with displacement,

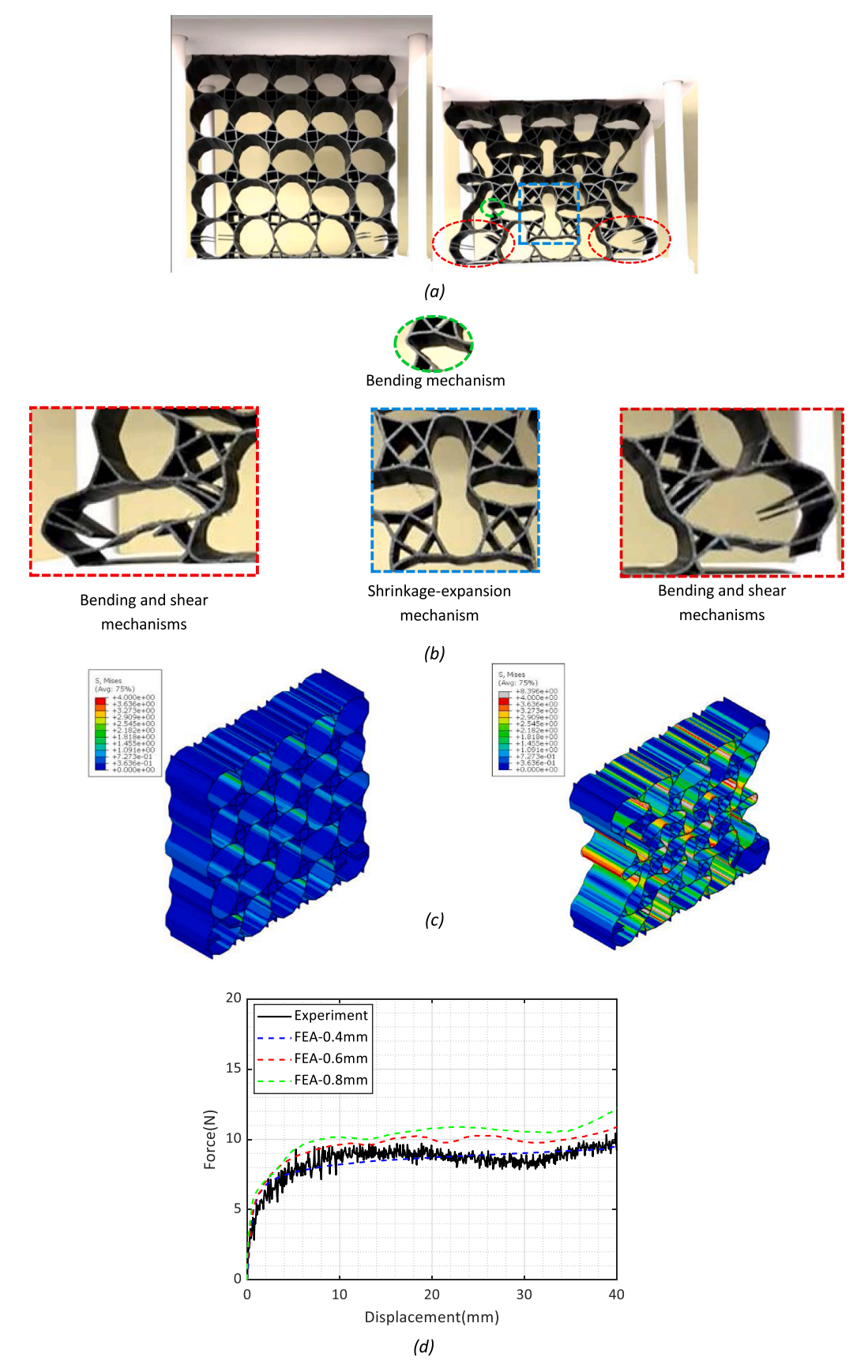


Fig. 11. (a) Quasi-static compression test on hierarchical triangular metamaterial, (b) existing deformation mechanisms, (c) stress distribution, and (d) FEA verification.

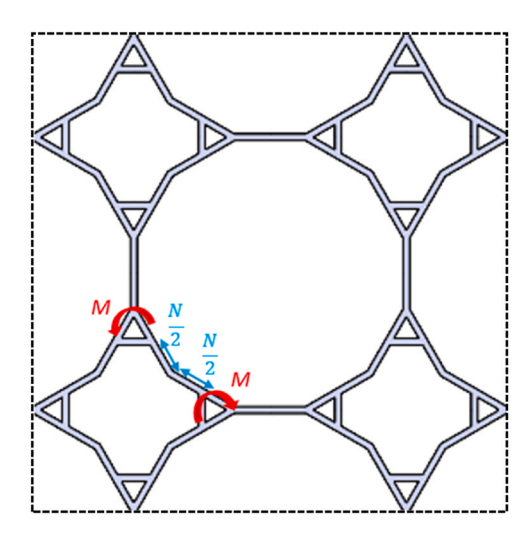


Fig. 12. Schematic representation of double half-length ligaments subjected to equal and opposite end moments "M".

which is a characteristic of positive stiffness response. This means that the hierarchical design introduces localized deformation mechanisms, particularly rotational and bending interactions concentrated around the triangular joints, resulting in QZS property. In fact, activating the rotating-bending mechanism under compression introduces nonlinearity into the system, resulting in a reduction of structural stiffness. In contrast, the dodecagon metamaterial lacks such a mechanism under compression; therefore, its stiffness remains almost unchanged, and no QZS behaviour is exhibited.

Although the vibration-isolated mass capacity varies with triangle support sizes, the QZS property and deformation pattern of the unit cells remain similar. To show the vibration isolation and energy generation features, the metamaterial with large triangles is considered as a case study, which will be described and explained in the following sections.

3.3. Vibration isolation feature

Fig. 14a demonstrates that embedding smart materials into the metamaterial structure, made up of five repeating unit cells along the horizontal and vertical directions "5 \times 5", leads to a significant increase in overall stiffness. After embedding of piezo materials, the structure exhibits notably higher stiffness across the entire displacement range compared to the non-embedded "5 \times 5" structure. Despite this increase in stiffness, the structure preserves its characteristic nonlinear deformation behaviour under compression. The reason for performing the vibration test on the structure with large triangles is that it has a lower QZS level, which eases the experiment due to the required lower mass to gain QZS property, and a longer plateau region compared to the structure with small triangles, see Fig. 13d. It is also worth mentioning that by repeating the unit cells three times along the horizontal and vertical directions " 3×3 ", while considering all geometrical constraints such as wall thickness and unit cell size constant, the hierarchical metamaterial containing large triangles can still provide QZS behaviour, see Fig. 14a. In terms of vibration isolation behaviour, all structures exhibit almost a similar pattern, see Fig. 14b, c, and d. Although the three designs differ, their first resonance occurs at nearly the same frequency. This is because we maintained a balance between structural stiffness and the attached mass, ensuring that the system reaches the QZS deformation stage under similar conditions. When this balance is preserved, the first resonance peak remains almost the same. The second resonance, however, does not necessarily align with the force-displacement response. Instead, it is governed by the internal deformation mechanisms of the metamaterial, which are particularly complex in soft TPU structures. This behaviour depends on the detailed geometry and deformation mode rather than

only the global stiffness observed in the force-displacement curve. Consequently, the second resonance frequency shifts with increasing stiffness, being highest for the "5 × 5" lattice with piezo, followed by the "5 × 5" without piezo, and lowest for the "3 × 3" design. In addition, high-amplitude components present in the base vibrations are effectively damped in the top plate, resulting in a more harmonic response, see Fig. 14e. It is worth mentioning that vibration suppression with embedded piezo materials occurs at 10.1562 Hz, where |Ta(f)| < 1, while without embedded piezo materials exhibits vibration suppression at 11 Hz.

3.4. Electricity generation and maximum generated power

The results in this section are provided based on the frequency domain and time domain from 0 to 0.5 seconds at 16 Hz. From Fig. 15a, it can be inferred that all piezo elements contribute to significant electricity generation below 20 Hz. The maximum electricity generated by PB is 7.67 $\frac{V}{g}$ at 1.5 Hz, by a piezo stack is 1.2 $\frac{V}{g}$ at 7 Hz, by "PZT left" is 0.5 $\frac{V}{g}$ at 6 Hz, and by "PZT right" is 0.08 $\frac{V}{g}$ at 16 Hz. The significant difference in generated voltage by "PZT left" and "PZT right" is caused by an imbalance of structural deformation due to highly flexible behaviour of TPU, probable imperfections related to printing, and imperfectly balanced dynamic loads during the vibration test, which leads to more twisting deformation patterns in the area of the metamaterial, where "PZT left" is embedded, see Fig. 15d. In addition, another reason is related to the PB embedment near the "PZT left". Once embedded, the PB introduced an increase in local stiffness in the area of the "PZT left". This leads to transferring more load on the PZT patch, resulting in higher voltage output compared to the "PZT right" without any PB nearby. It is also worth mentioning that the higher voltage output at low frequencies can be attributed to the placement of the piezoelectric elements near the shaker, where they are exposed to stronger external excitations. Apart from that, vibration isolation behaviour arises at 10 Hz onwards, see Fig. 14b, leading to lower electricity generation at 20 Hz onwards due to dampening the effective excitations applied to piezo elements. The same power generation trend can be seen from Fig. 15b, meaning that at low frequencies below 10 Hz, significant power generation by the piezo elements exists. However, at 10.1562 Hz, where vibration isolation arises, PB generates a power of $8.6 \frac{\mu W}{g}$, and the piezo stack generates $2.6 \frac{\mu W}{g}$ of power. This approves the multifunctionality of the proposed hierarchical triangular metamaterials, showing simultaneous vibration isolation, reasonable electricity and power generation at around 10 Hz onwards. On this matter, Fig. 15c shows the history of voltage generation by piezo elements at 16 Hz. It is worth mentioning that PZT elements generate more power at high frequencies compared to low frequencies.

3.5. Potential applications

Considering that typical sensors need a power of $10\text{--}1000~\mu\text{W}$ to operate [64], the generated power by a single piezo bender and piezo stack in this research is already within the usable range for intermittent operation. It is worth mentioning that the structural design allows for multiple piezo benders to be embedded in a whole layer of the lattice, enabling scalable power output for more demanding applications. Therefore, the proposed hierarchical metamaterials offer a promising solution for both effective vibration isolation and self-powered sensor integration in practical applications. Since they are fabricated from soft TPU and begin to exhibit effective vibration isolation from 10.1562 Hz onwards, they present a promising solution for integration into shoes, see Fig. 16a. More importantly, workers operating heavy machinery or vibrating tools are often exposed to low-frequency excitations in the range of 10–60 Hz, which can lead to discomfort, fatigue, and long-term musculoskeletal disorders [65]. By embedding the metamaterial within

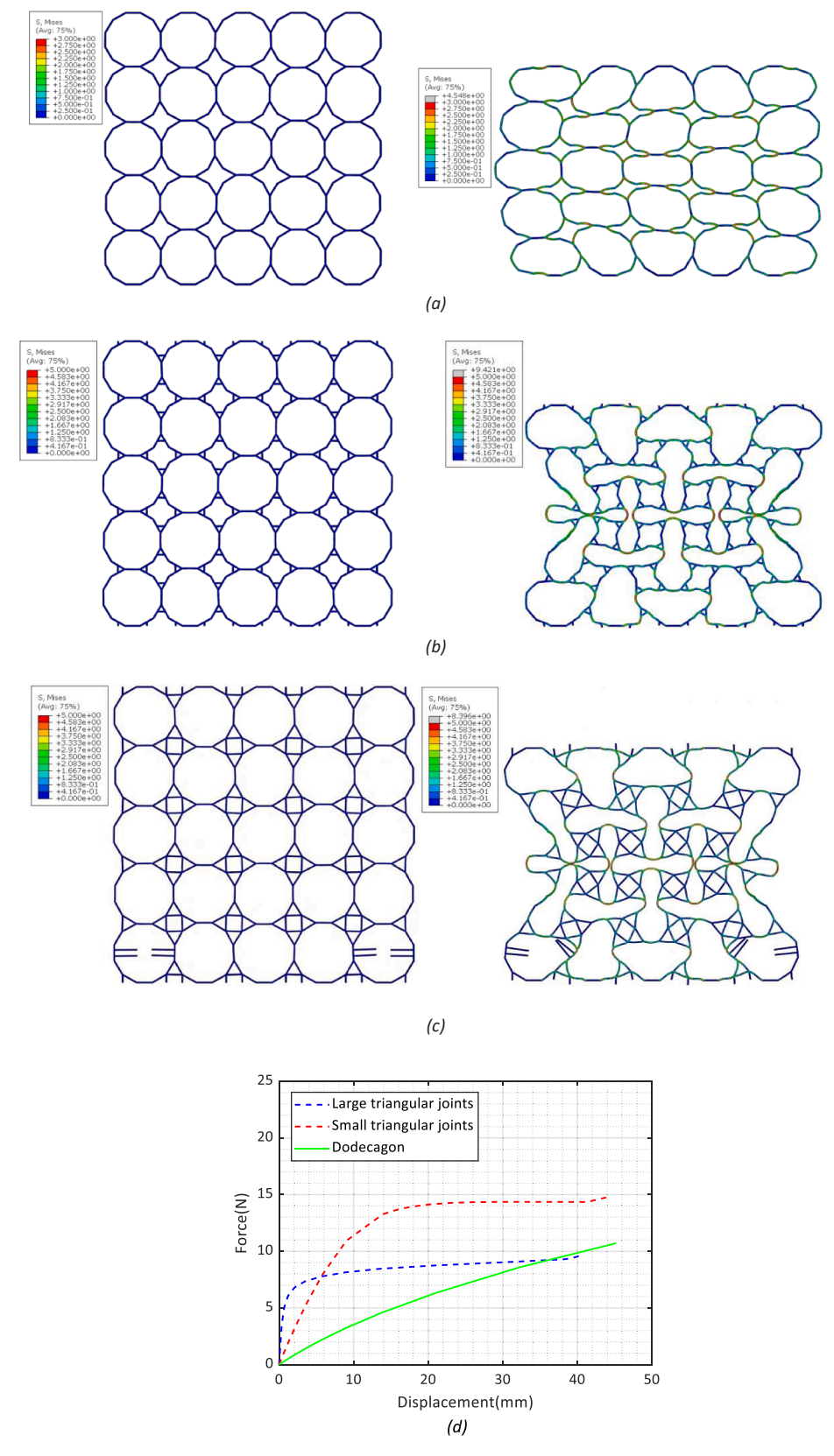


Fig. 13. (a) Deformation patterns of the dodecagon, (b) hierarchical metamaterial with small triangles, (c) hierarchical metamaterial with large triangles and (d) the corresponding force-displacement response obtained from FEA.

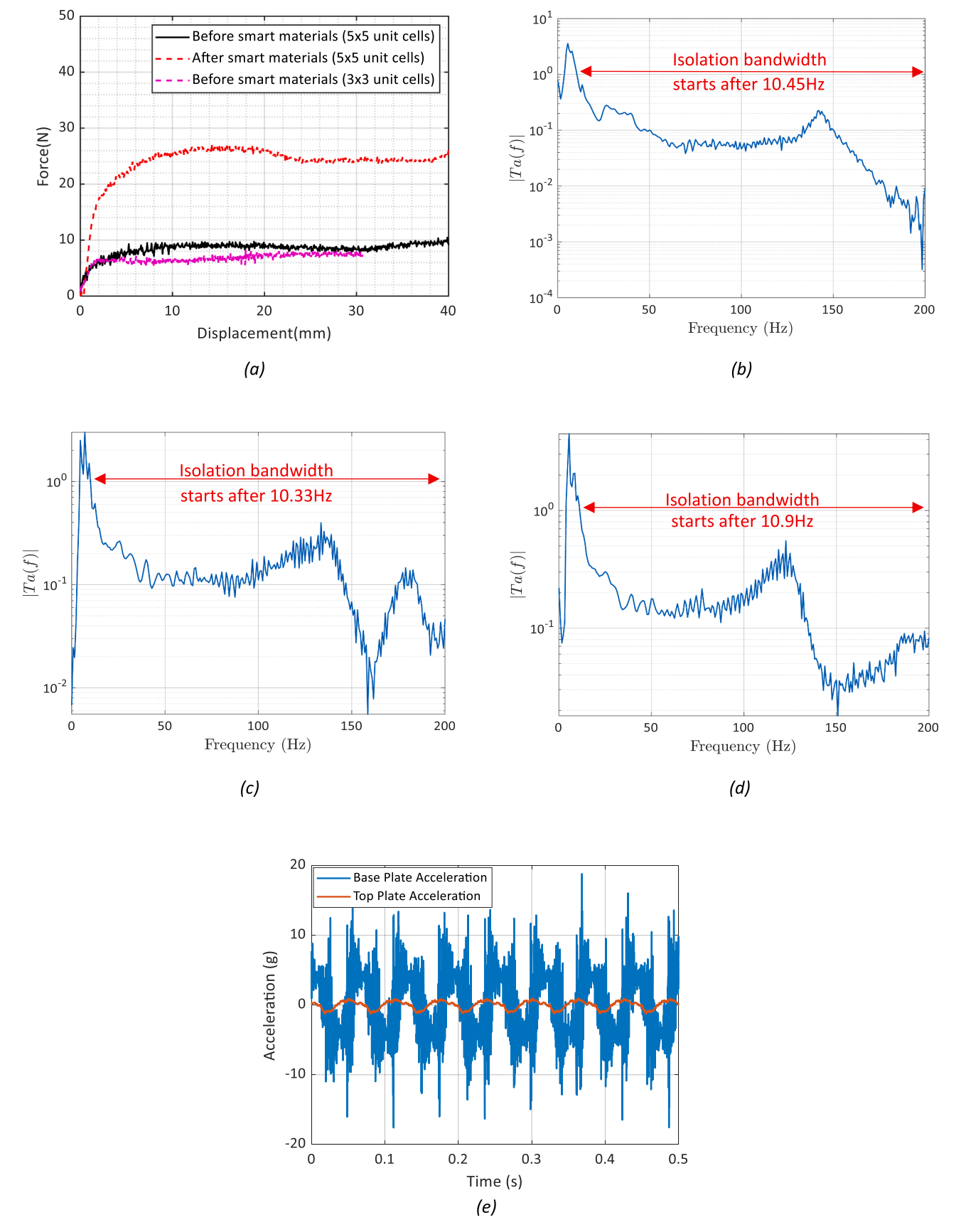


Fig. 14. (a) The embedding effect of smart materials on force-displacement response, (b) transfer function (normalized output acceleration per gravity) of large triangular metamaterials with embedded smart materials " 5×5 ", (c) without smart materials " 5×5 ", (d) without smart materials " 3×3 ", and (e) time-domain response of hierarchical metamaterial with embedded smart materials " 5×5 ".

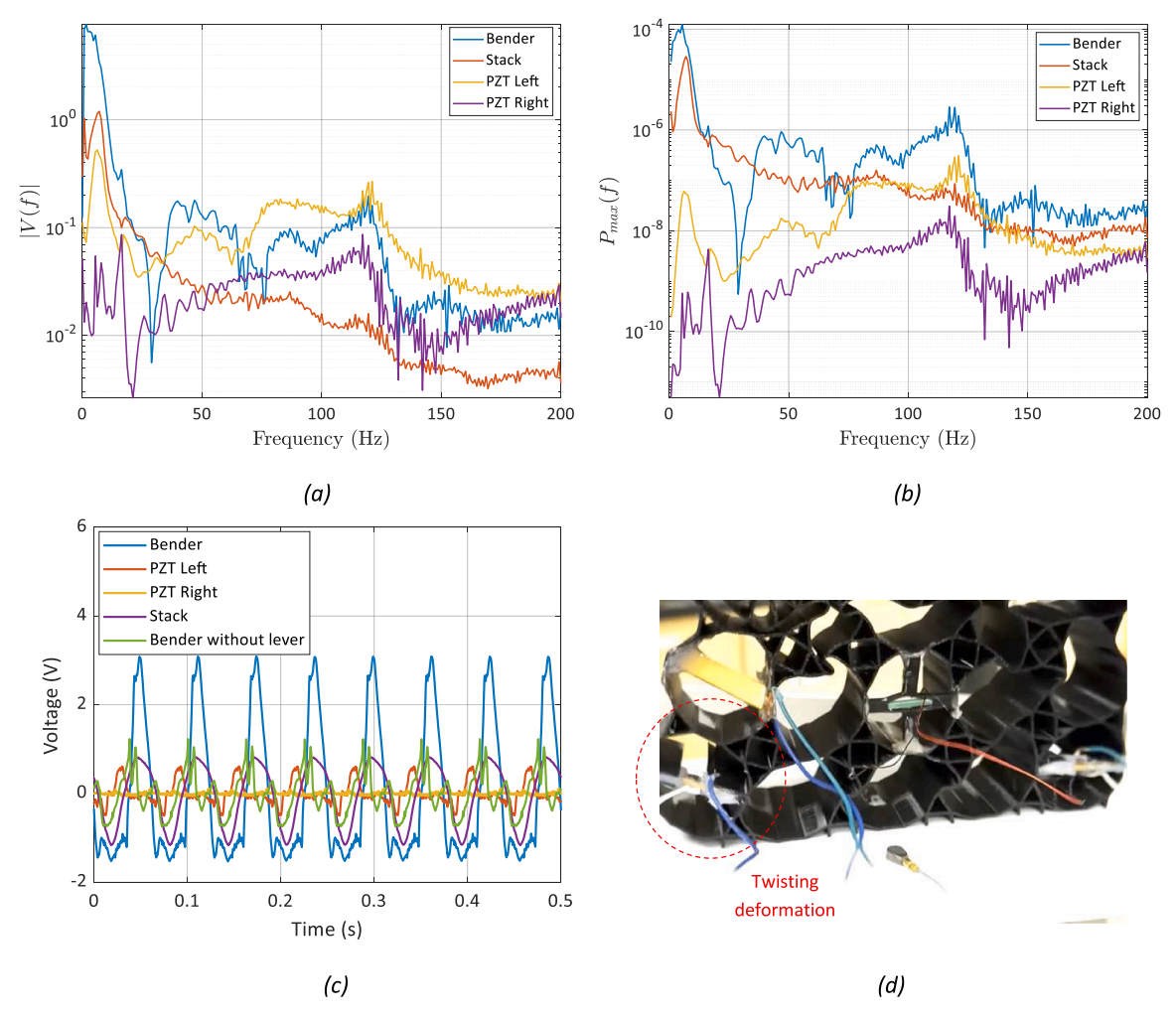


Fig. 15. (a) Voltage transfer function (normalized per gravity), (b) power transfer function, (c) time-domain generated voltage at 16 Hz, and (d) twisting deformation happens in the area of "PZT left".

the heel or mid-sole of the shoes/boots, harmful ground-transmitted vibrations can be effectively attenuated, thereby improving runner/worker comfort and safety. Simultaneously, the embedded piezo elements enable continuous low-power energy harvesting during routine activities. This harvested energy can be directed to heat thin-film elements embedded within the shoe/boot lining, offering thermal comfort in cold environments such as harsh Canadian winters. A similar example can be a pneumatic hammer drill or jackhammers, see Fig. 16b. Drill operators are regularly exposed to intense low-frequency vibrations. By integrating the metamaterial directly into the handle grip area, the lattice can act as a localized isolator, significantly reducing transmitted vibration to the operator's hands and arms. The use of flexible TPU ensures that the embedded structure remains lightweight, compliant, and well-suited for prolonged wear, supporting both biomechanical performance and self-powered functionality. Additionally, the proposed metamaterial can be employed beneath large vibrating appliances, such as washing machines or dryers, see Fig. 16c, where low-frequency vibrations ranging from 8 to 50 Hz are commonly observed during operation. Conventional rubber pads provide limited isolation and often degrade over time. In contrast, the QZS behaviour of the hierarchical structure enables effective attenuation of harmful ground-transmitted vibrations, minimizing structural noise, floor damage, and machine wear. Beyond industrial and mobility applications, the proposed metamaterial can also serve as a smart fall detection pad for elderly individuals, see Fig. 16d. When integrated into protective wear or flooring, the structure not only attenuates the impact force, but also

enables self-powered sensing of fall incidents. Upon experiencing a high-deformation incident such as a fall, the embedded piezoelectric elements generate a voltage signal that can be wirelessly transmitted to local health services such as the Manitoba Clinic, enabling timely medical intervention. This approach offers a battery-free, real-time alert system to improve elderly safety.

3.6. Fatigue durability

Following the potential applications mentioned in Section 3.5, the fatigue durability of the proposed metamaterials is evaluated in this section. On this matter, the viscoelasticity of the "5 × 5" TPU-based metamaterial with embedded piezoelectric elements is examined under realistic conditions. For this purpose, the frequency-response curve of the "5 × 5" metamaterial with embedded piezo elements is considered, see Fig. 14b. To calculate the damping ratio and loss factor, the "half power bandwidth" method is used [30]. The half-power bandwidth method is an experimental technique to determine the damping ratio, ζ , of a system by analyzing its frequency-response function, as in Eq. (11). Indeed, in the half-power bandwidth method, the damping ratio is determined by identifying the two frequencies, f_1 and f_2 , on either side of the resonance peak, f_n , where the system's response amplitude drops to $\frac{1}{\sqrt{2}}$. Loss, η , and dynamic magnification, M, factors are calculated as Eqs. (12) and (13), respectively.

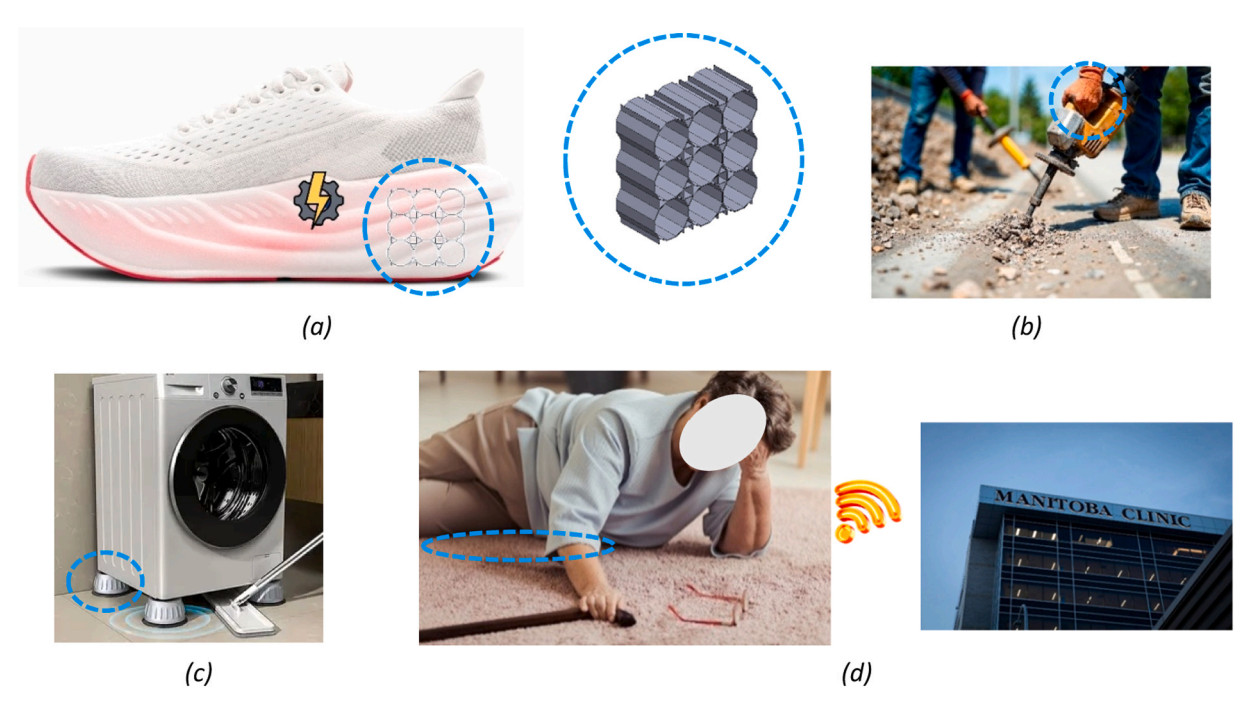


Fig. 16. (a) attachment of proposed hierarchical metamaterials in the shoe mid-sole, (b) drill handle, (c) bases of washing/dryer machine to isolate vibration and simultaneously power-up heating/electrical elements, and (d) smart fall protection-detection flooring.

$$\zeta = \frac{f_2 - f_1}{2f_n} \tag{11}$$

$$\eta = \frac{\zeta}{2\pi} \tag{12}$$

$$M = \frac{1}{2\zeta\sqrt{1-\zeta^2}} \tag{13}$$

According to the equations mentioned above, the calculated values are as follows: $\zeta = 0.38$, $\eta = 0.06$, and M = 1.42. The calculated damping ratio, $\zeta = 0.38$, demonstrates that the TPU-based metamaterial possesses strong structural damping under dynamic loading. The dynamic magnification factor, M = 1.42, indicates that the maximum vibration amplitude at resonance is approximately 1.4 times greater than the static condition. The corresponding loss factor, $\eta = 0.06$, implies that approximately 6 % of the stored elastic energy is dissipated as heat during each loading cycle, confirming the intrinsic viscoelastic nature of the material. Indeed, the relatively small hysteretic loss reflects the super-reversible and low-hysteresis nature of the TPU-based metamaterial, which recovers its deformation upon unloading while dissipating only a limited fraction of energy through molecular friction. Consequently, the combination of a high damping ratio and moderate loss factor indicates that the TPU matrix efficiently converts mechanical energy into thermal dissipation, reducing local stress concentrations and delaying crack initiation during repeated loading. Another important item which must be considered is related to the viscoelastic property of the glue under dynamic loads used for bonding the piezoelectric elements to the TPU-based metamaterial. On this matter, we used the "EVA" glue stick [66] in this research, showing glue modulus varies from 0.1 MPa to 10 MPa, which is under (close) to the stiffness of the TPU material at low strains. Therefore, the bonding areas in this research remained unaffected under realistic dynamic conditions. In addition, it is also worth noting that because of the flexibility of the TPU and its excellent vibration-damping properties, no fracture was seen on the piezoelectric elements.

4. Conclusion

This study developed additively manufactured TPU-based hierarchical triangular metamaterials designed for simultaneous vibration isolation and electricity generation. The main findings are summarized as follows.

- The introduction of a rotation-bending mechanism through triangular supports between dodecagon cells effectively induces a quasizero-stiffness (OZS) property.
- The level of QZS property is tunable. The larger the triangles, the lower the force value corresponding to the QZS and earlier yield, vice versa.
- The presence of local deformation mechanisms such as pure bending, bending-shear, and expansion-compression enables the integration of suitable piezoelectric elements for energy harvesting.
- The proposed metamaterial exhibits low-frequency vibration isolation from approximately 10.15 Hz onward, with consistent performance regardless of unit-cell repetition.
- 5. At low frequencies where vibration isolation arises, the piezo bender and piezo stack generate power around 8.6 $\frac{\mu W}{g}$ and 2.6 $\frac{\mu W}{g}$ respectively, while PZT generates power around 1 $\frac{nW}{g}$.
- 6. At a high frequency of 200 Hz, the piezo bender generates a power of $32 \, \frac{nW}{g}$, piezo stack generates a power of 7.6 $\frac{nW}{g}$, and PZT generates a power of 2.9 $\frac{nW}{g}$.

It is worth noting that embedding heating elements within the metamaterial could lower the damped natural frequency. Meanwhile, the electricity generated by the embedded piezoelectric elements during vibration can be harvested through an energy-conditioning circuit consisting of a rectifier, storage capacitor, and voltage regulator. The stored energy can then be utilized to power low-energy electronic devices, enabling self-sustained operation. The multifunctional capabilities of the proposed metamaterials open new avenues for practical implementation in both wearable and industrial settings. Their ability to isolate low-frequency vibrations (from 10.15 Hz onwards) while simultaneously generating usable electrical power makes them ideal for

enhancing worker comfort and safety. These structures can be embedded into shoes or boots, or integrated with power tools to reduce vibration exposure and support self-powered sensing and control systems. This proposed concept highlights a promising pathway toward next-generation multifunctional metamaterial vibration isolators.

CRediT authorship contribution statement

Mahdi Bodaghi: Writing – review & editing, Supervision, Software, Methodology, Investigation. Nan Wu: Writing – review & editing, Supervision, Methodology, Conceptualization. Ramin Hamzehei: Writing – original draft, Validation, Software, Methodology, Investigation, Formal analysis, Conceptualization. Mahdi Alaei Varnosfaderani: Writing – original draft, Validation, Software, Methodology, Investigation, Formal analysis.

Declaration of Competing Interest

The authors declare that they have no known competing financial interests or personal relationships that could have appeared to influence the work reported in this paper.

Acknowledgements

The authors would like to gratefully acknowledge the support by the University of Manitoba, National Sciences and Engineering Research Council of Canada [NSERC, RGPIN 2021–03356], Mitacs Accelerate [IT45842], and the UK Engineering and Physical Sciences Research Council (EPSRC) [award number: EP/Y011457/1].

Appendix A. Supporting information

Supplementary data associated with this article can be found in the online version at doi:10.1016/j.sna.2025.117230.

Data availability

Data will be made available on request.

References

- [1] C. Perez-Garcia, R. Zaera, J. Aranda-Ruiz, G. Bordiga, G. Risso, M.L. Lopez-Donaire, et al., Reprogrammable mechanical metamaterials via passive and active magnetic interactions, Adv. Mater. (2025) 2412353.
- [2] R. Hasanzadeh, S. Jolaiy, M. Mojaver, T. Azdast, C.B. Park, Auxetic 3D printed metastructure stents for enhanced mechanical and structural performance and biocompatibility in coronary artery treatments, Acta Biomater. (2025).
- [3] X. Tan, S. Zhu, B. Wang, M. Kadic, Tuning negative stiffness mechanical metamaterial's snap-through behavior with a series-connected spring, Eur. J. Mech. A Solids 107 (2024) 105382.
- [4] C. Zhang, F. Lu, T. Wei, H. Wang, F. Liu, Y. Zhu, Windmill-shaped metamaterials achieving negative thermal expansion, Eng. Struct. 336 (2025) 120488.
- [5] Y. Lyu, X. Song, H. Wang, J. Jiang, A novel mechanical metamaterial with tunable stiffness and individually adjustable poisson's ratio, Mater. Today Commun. 40 (2024) 110135.
- [6] X. Song, C. Zeng, J. Hu, W. Zhao, L. Liu, Y. Liu, J. Leng, Compressive behavior and energy absorption of novel body-centered cubic lattice metamaterials incorporating simple cubic truss units. Compos. Struct. (2025) 119230.
- [7] Y. Liu, Mechanical properties of a new type of plate–lattice structures, Int. J. Mech. Sci. 192 (2021) 106141.
- [8] Y. Wang, K. Wu, X. Zhang, X. Li, Y. Wang, H. Gao, Superior fracture resistance and topology-induced intrinsic toughening mechanism in 3D shell-based lattice metamaterials, Sci. Adv. 10 (35) (2024) eadq2664.
- [9] R. Hamzehei, M. Bodaghi, N. Wu, 3D-printed highly stretchable curvy sandwich metamaterials with superior fracture resistance and energy absorption, Int. J. Solids Struct. 286 (2024) 112570.
- [10] E. Bahmanpour, A. Montazeri, A. Saeedi, M. Mahnama, Flexural behaviors of asymmetric Re-entrant auxetic honeycombs, Eur. J. Mech. A/Solids 109 (2025) 105475.
- [11] W. Wu, D. Qi, H. Liao, G. Qian, L. Geng, Y. Niu, J. Liang, Deformation mechanism of innovative 3D chiral metamaterials, Sci. Rep. 8 (1) (2018) 12575.

- [12] R. Hamzehei, S. Rezaei, J. Kadkhodapour, A.P. Anaraki, A. Mahmoudi, 2D triangular anti-trichiral structures and auxetic stents with symmetric shrinkage behavior and high energy absorption, Mech. Mater. 142 (2020) 103291.
- [13] D. Mousanezhad, B. Haghpanah, R. Ghosh, A.M. Hamouda, H. Nayeb-Hashemi, A. Vaziri, Elastic properties of chiral, anti-chiral, and hierarchical honeycombs: A simple energy-based approach, Theor. Appl. Mech. Lett. 6 (2) (2016) 81–96.
- [14] S. Akram, A. Israr, Passive Acoustic Metamaterials for Low Frequencies—Theories, Types, Testing, and Future Directions, Adv. Eng. Mater. 27 (5) (2025) 2402270.
- [15] S. Xiao, T. Wang, T. Liu, C. Zhou, X. Jiang, J. Zhang, Active metamaterials and metadevices: a review, J. Phys. D Appl. Phys. 53 (50) (2020) 503002.
- [16] J. Rossiter, K. Takashima, F. Scarpa, P. Walters, T. Mukai, Shape memory polymer hexachiral auxetic structures with tunable stiffness, Smart Mater. Struct. 23 (4) (2014) 045007.
- [17] D. Dengiz, H. Goldbeck, S.M. Curtis, L. Bumke, J. Jetter, E. Quandt, Shape memory alloy thin film auxetic structures, Adv. Mater. Technol. 8 (12) (2023) 2201991.
- [18] R. Ahamed, S.-B. Choi, M.M. Ferdaus, A state of art on magneto-rheological materials and their potential applications, J. Intell. Mater. Syst. Struct. 29 (10) (2018) 2051–2095.
- [19] Y. Xiao, Q. Han, N. Wu, Piezoelectric energy harvesting: a review of energy sources, structures, and working mechanisms in high-frequency excitations and operations, Smart Mater. Struct. (2025).
- [20] J. Liu, J. Liu, K. Gao, I. Mohagheghian, W. Fan, J. Yang, Z. Wu, A bioinspired gradient curved auxetic honeycombs with enhanced energy absorption, Int. J. Mech. Sci. 291 (2025) 110189.
- [21] J. Lee, H. Lim, J. Park, J. Lee, D. Noh, S. Jiong, et al., Data-driven design of lightweight, interface-free metamaterial composites tailored for enhanced broadband electromagnetic absorption with robust mechanical properties, Compos. Part B Eng. (2025) 112838.
- [22] X. Wang, T. Fu, A novel arc-type auxetic cellular doubly-curved shells with negative Poisson's ratio for broadband low-frequency sound insulation, Eur. J. Mech. A/Solids 106 (2024) 105326.
- [23] Z. Liang, C. Liu, Y. Liu, Y. Ma, F. Ma, Demand-driven inverse design and optimization for ultra-thin broadband sound-absorbing metamaterials based on metaheuristic-enhanced autoencoder network, Composites Part B Engineering (2025) 112643.
- [24] L. Meng, M. Zhong, Y. Gao, T. Gao, Y. Hou, J. Zhu, et al., Impact resisting mechanism of tension-torsion coupling metamaterials, Int. J. Mech. Sci. 272 (2024) 109100.
- [25] Y. Lu, X. Feng, S. Fu, S. Ma, S. Fu, S. Zheng, et al., Multidimensional Twisted Mechanical Metamaterials with Programmable Stiffness for Adaptive Impact Protection, Composites Part B Engineering (2025) 112848.
- [26] R. Hamzehei, M. Bodaghi, N. Wu, Mastering the art of designing mechanical metamaterials with quasi-zero stiffness for passive vibration isolation: A review, Smart Mater. Struct. (2024).
- [27] L. Xu, Z. Yang, Z. Zhang, E. Li, J. Zhou, B. Li, Lightweight composite meta-lattice structures with inertial amplification design for broadband low-frequency vibration mitigation, Compos. Part B Eng. 292 (2025) 112091.
- [28] W.J. Ferguson, Y. Kuang, K.E. Evans, C.W. Smith, M. Zhu, Auxetic structure for increased power output of strain vibration energy harvester, Sens. Actuators A Phys. 282 (2018) 90–96.
- [29] Q. Li, T. Wu, W. Zhao, Y. Li, J. Ji, G. Wang, 3D printing stretchable core-shell laser scribed graphene conductive network for self-powered wearable devices, Compos. Part B Eng. 240 (2022) 110000.
- [30] S.S. Rao, F.F. Yap, Mechanical vibrations, Addison-Wesley, New York, 1995.
- [31] J. Ji, Q. Luo, K. Ye, Vibration control based metamaterials and origami structures: a state-of-the-art review, Mech. Syst. Signal Process. 161 (2021) 107945.
- [32] G. Pan, X. Jiao, C. Lin, Z. Guan, J. Wu, H. Liu, et al., High Load-Bearing Quasi-Zero Stiffness Metamaterials for Vibration Isolation, Int. J. Mech. Sci. 293 (2025) 110225.
- [33] X. Liu, S. Chen, B. Wang, X. Tan, A multi-dimensional quasi-zero-stiffness mechanical metamaterial with different directional vibration isolation capabilities, Smart Mater. Struct. 34 (4) (2025) 045013.
- [34] L. Li, F. Yang, S. Liu, Z. Guo, D. Han, Y. Xia, et al., Design of quasi-zero-stiffness metamaterials with ultra-wideband vibration isolation performance, Int. J. Mech. Sci. (2025) 110440.
- [35] P. Wu, S. Li, Z. Li, W. Xia, Y. Li, Modular QZS metamaterials with enhanced load adaptability for low-frequency vibration isolation, Smart Mater. Struct. 34 (5) (2025) 055017.
- [36] W. Liu, L. Wu, J. Zhang, J. Sun, J. Zhou, Metamaterial springs for low-frequency vibration isolation, J. Mater. 11 (1) (2025) 100884.
- [37] S. Dalela, B. PS, D.P. Jena, M. Leblouba, A tunable metamaterial using a single beam element with quasi-zero-stiffness characteristics for low-frequency vibration isolation, J. Vib. Control 30 (15-16) (2024) 3641–3658.
- [38] X. Liu, S. Chen, X. Tan, S. Li, B. Wang, A mechanical metamaterial with programmable arbitrary quasi-zero-stiffness regions, Compos. Part A Appl. Sci. Manuf. (2025) 109076.
- [39] K. Huo, Z. Yuan, G. Zhou, R. Mu, K. Wang, H. Zhao, Modeling of programmable low-frequency isolator with quasi-zero stiffness metamaterials, Acta Mech. 235 (5) (2024) 2919–2944.
- [40] C. Ma, K. Wu, Y.-F. Wang, Y.-S. Wang, Customized design of periodic metacushion with quasi-zero-stiffness for low-frequency vibration isolation, Int. J. Solids Struct. (2025) 113518.
- [41] Z. Zhang, Z. Qi, D. Pan, Design and test of a quasi-zero stiffness metastructure based on the preshaped beams for low-frequency vibration isolation, Mater. Des. 253 (2025) 113853.

- [42] L. Xu, Z. Xiang, Compliant quasi-zero stiffness device for vibration energy harvesting and isolation, Sens. Actuators A Phys. 347 (2022) 113964.
- [43] Q. Zhang, D. Guo, G. Hu, Tailored mechanical metamaterials with programmable quasi-zero-stiffness features for full-band vibration isolation, Adv. Funct. Mater. 31 (33) (2021) 2101428.
- [44] X. Zhang, X. Shan, G. Sui, C. Hou, X. Du, Z. Min, T. Xie, Enhancing piezoelectric energy harvesters with rotating triangular auxetic structures, Int. J. Mech. Sci. 289 (2025) 110081.
- [45] N. Mortazavi, S. Ziaei-Rad, Energy harvesting from vibrations of a beam under mass passage by arc-shaped auxetic cantilever beams, Eur. J. Mech. A/Solids 109 (2025) 105432.
- [46] F.Ç. Bolat, A. Sugeç, A. Özdemir, Design, numerical analysis and experiments of different types auxetic beams for vibration based energy harvester, Mech. Syst. Signal Process. 210 (2024) 111170.
- [47] H. Zhang, S. Chen, M. Karimi, B. Li, S. Saydam, M. Hassan, Numerical and experimental investigation of an auxetic piezoelectric energy harvester with frequency self-tuning capability, Smart Mater. Struct. 33 (5) (2024) 055022.
- [48] M. Ravanbod, S. Ebrahimi-Nejad, Perforated auxetic honeycomb booster with reentrant chirality: a new design for high-efficiency piezoelectric energy harvesting, Mech. Adv. Mater. Struct. 31 (27) (2024) 9857–9872.
- [49] A. Megdich, M. Habibi, L. Laperrière, Z. Li, Y. Abdin, Enhanced piezoelectric performance of PVDF/MWCNTs energy harvester through a 3D-printed multimodal auxetic structure for smart security systems, Mater. Today Sustain. 27 (2024) 100847.
- [50] R. Ichige, N. Kuriyama, Y. Umino, T. Tsukamoto, T. Suzuki, Size optimization of metamaterial structure for elastic layer of a piezoelectric vibration energy harvester, Sens. Actuators A Phys. 318 (2021) 112488.
- [51] L. Zhao, Z. Lu, H. Ding, L. Chen, A viscoelastic metamaterial beam for integrated vibration isolation and energy harvesting, Appl. Math. Mech. 45 (7) (2024) 1243–1260.
- [52] S. Fang, H. Du, T. Yan, K. Chen, Z. Li, X. Ma, et al., Theoretical and experimental investigation on the advantages of auxetic nonlinear vortex-induced vibration energy harvesting, Appl. Energy 356 (2024) 122395.
- [53] N. Mortazavi, S. Ziaei-Rad, Energy harvesting from vibrations of a beam under moving mass using auxetic cantilever beams: theoretical and experimental investigations, Mech. Adv. Mater. Struct. 32 (5) (2025) 991–1027.
- [54] K. Chen, S. Fang, Z. Lai, J. Cao, W.-H. Liao, A plucking rotational energy harvester with tapered thickness and auxetic structures for increasing power output, Appl. Energy 357 (2024) 122490.
- [55] J. Wang, Y. Zhang, Z. Chen, C. Wang, S.-K. Lai, Exploring the impact of auxetic structures in a hybrid design approach to low-frequency vibration energy harvesting, Smart Mater. Struct. 34 (6) (2025) 065005.
- [56] C. Liu, R. Zhao, K. Yu, H.P. Lee, B. Liao, A quasi-zero-stiffness device capable of vibration isolation and energy harvesting using piezoelectric buckled beams, Energy 233 (2021) 121146.
- [57] C. Liu, J. Wang, W. Zhang, X.-D. Yang, X. Guo, T. Liu, X. Su, Synchronization of broadband energy harvesting and vibration mitigation via 1: 2 internal resonance, Int. J. Mech. Sci. (2025) 110503.
- [58] R. Hamzehei, J. Kadkhodapour, A.P. Anaraki, S. Rezaei, S. Dariushi, A. M. Rezadoust, Octagonal auxetic metamaterials with hyperelastic properties for large compressive deformation, Int. J. Mech. Sci. 145 (2018) 96–105.
- [59] H.J. Qi, M.C. Boyce, Stress-strain behavior of thermoplastic polyurethanes, Mech. Mater. 37 (8) (2005) 817–839.

- [60] A. Standard, Standard test method for tensile properties of plastics, ASTM Int. Des. D. 638 (2003) 1–13.
- [61] Available from: https://www.piezodrive.com/actuators/piezo-bender-actuators/.
- [62] I. Pandiev, N. Tomchev, N. Kurtev, M. Aleksandrova, Analysis of the methods for realization of low-power piezoelectric energy harvesting circuits for wearable battery-free power supply devices, Applied Sciences 14 (11) (2024) 4792.
- [63] F.P. Beer, E.R. Johnston Jr, J.T. DeWolf, D.F. Mazurek, Mechanics of materials, McGraw Hill (2006).
- [64] R. Hidalgo-Leon, J. Urquizo, C.E. Silva, J. Silva-Leon, J. Wu, P. Singh, G. Soriano, Powering nodes of wireless sensor networks with energy harvesters for intelligent buildings: A review, Energy Reports 8 (2022) 3809–3826.
- [65] K. Krajnak, Health effects associated with occupational exposure to hand-arm or whole body vibration, Journal of Toxicology and Environmental Health, Part B 21 (5) (2018) 320–334.
- [66] M. Schubnell, Investigation of the curing reaction of EVA by DSC and DMA, Photovoltaics International 7 (2010) 131–137.

Ramin Hamzehei is a Ph.D. candidate in Mechanical Engineering at the University of Manitoba, Canada, under the supervision of Prof. Nan Wu. His research focuses on the design and characterization of mechanical metamaterials and lattice structures for multifunctional applications, including energy absorption/dissipation, vibration isolation, and energy harvesting. He has collaborated with several international researchers and published multiple papers in leading journals on smart and tunable metamaterials. His current work explores the integration of piezoelectric materials within metamaterials for simultaneous vibration control and energy harvesting.

Mahdi Alaei, Ph.D. His research interests lie in mechanical vibrations, acoustics, vibration isolation, resonant drilling, and energy harvesting systems. His work integrates experimental and computational methods to develop smart and efficient vibro-mechanical structures for advanced engineering applications.

Mahdi Bodaghi is Associate Professor of Smart Materials & Manufacturing in the Department of Engineering at Nottingham Trent University. He is also the founder and director of the 4D Materials & Printing Lab that develops electro/magneto/thermoresponsive materials, resilient metamaterials, sustainable bio-composites, and 3D/4D printing technologies. His experience and research have led him to co-found the 4D Printing Society, to co-edit Elsevier book series-Smart Materials in Additive Manufacturing, and to launch 4D Printing Journal. His research has been disseminated through over 340 peer-reviewed papers in prestigious journals as well as the presentation at international conferences (Google Scholar, Citations: 13660, h-index: 67).

Dr. Nan Wu obtained his B.Eng and M.Sc from Northeastern University China in 2005 and 2008, respectively, and received his Ph.D. degree in 2012 from the University of Manitoba. Currently, Dr. Nan Wu is working as a full Professor in the Department of Mechanical Engineering – at the University of Manitoba with teaching and research interests in the fields of Mechanical Vibration, Smart Materials, Metamaterials, Nano-technology, and their applications to Condition Monitoring, Structural Enhancement, and Energy Harvesting with more than 110 journal paper published. Including the International Journal of Mechanical Sciences, Dr. Wu has served on the editorial boards of 6 international journals. He is a reviewer for more than 60 high-quality international journals.